Journal of Physics B: Atomic, Molecular and Optical Physics

The finding of transition-metal-doped binary superatoms: TM@Li15

To cite this article before publication: Li juan Yan 2019 *J. Phys. B: At. Mol. Opt. Phys.* in press https://doi.org/10.1088/1361-6455/ab470c

The finding of transition-metal-doped binary superatoms: TM@Li_{15}

*Lijuan Yan**
College of Electronics & Information Engineering, Guangdong Ocean University, Zhanjiang 524088, China
Corresponding Author *E-mail: ylj_gdou@126.com

As the first step of cluster-assembled materials, it is crucial to design stable clusters. In the paper, a type of D_{3h} symmetry 15-coordinate core-shell superatoms TM@Li_{15} is proposed by encapsulating a transition-metal atom (TM=Sc, Ti, Y, Zr, Nb, Hf, and Ta) into the Li_{15} cage, of which the center is located the assigned transition-metal atom. The unique structures are identified as the global minima though CALYSPO structure prediction method and frequency calculations. Energy calculations also confirm that they are very stable. Molecular orbital analysis reveals that all the D_{3h} symmetry isomers TM@Li_{15} (TM=Sc, Ti, Y, Zr, Nb, Hf, and Ta) are with the superatomic properties, where their stability can be well understand based on the superatom and magnetic superatom models. Our findings enrich the superatom family and may offer building units for cluster-assembling materials.

Keywords: the jellium model; superatoms; effective valance electrons; transition-metal doped; magnetic moment.

I. INTRODUCTION

In recent years, the research interests on atomic clusters are continuous increasing mainly due to two considerations. One is that the properties can be customized by selection of their compositions, shapes, sizes, and the charged states. Another is offering an amount of building blocks for cluster-assembled materials with tailor-made properties in specific applications [1-12]. As an example, the centered icosahedral Al_{13}^- is a cluster known for its pronounced stability, of which the characters are with a resemblance to a chloride ion [13]. By combining the neutral Al_{13} with superalkalis K_3O, Khanna and coworkers successfully design stable superatom assemblies $(Al_{13}K_3O)_n$ with tunable electronic features [7]. For the potential of industrial development, the almost completely spherical C_{60} cluster can be controlled forming materials in potential use of the field effect transistors [8-9] and solar cells [10-11]. The nanowires assembled from $M_{12}N_{12}$ (M = Al and Ga) clusters should be potential gas sensors for CO, NO, and NO_2 detection [12]. However, not all the clusters can be chosen as the building units, where the first and essential condition is possessing a high stability.

The stability of metal clusters can be understood by the jellium model [14-15], where the motions of valence electrons are subjected in a uniform positive charge background consisting of the atomic nuclei and the innermost electrons of the clusters. The filling orders of valence electrons in the metal clusters are $|1S^2|1P^6|1D^{10}2S^2|1F^{14}2P^6|$ …, and the electron counts of metal clusters with high stability are 2, 8, 18, 20, 34, 40, 58, etc., corresponding to the electronic shell closures.

According to the jellium model, the origin of high stability of 40-electron Al_{13}^- is due to its electronic shell closure. Such clusters with high stability are called superatoms, of which the valence electrons are confined in a series of shells with the shapes resembled to that of atomic orbitals and the chemical behaviour is analogous to the simple atoms in the periodic table. In 2009, the concept of superatom was extended to unpaired specices, where composite systems were assumed with some atoms offering the stability and others imparting their magnetic moments [16]. To demonstrate the possibility, an endohedral binary isolated cluster VCs_8 and a ligated $MnAu_{24}(SH)_{18}$ are chosen as examples. Since then, an amount of magnetic superatoms, especially binary clusters, are surged [17-21].

The particularly intriguing of endohedral binary superatom is that their properties can be designed by variation of the central dopants while the geometric structures are retained. Taking the superhalogen Al_{13} as an example, the centered aluminum atom is replaced by a C or P element, the icosahedrons are with the properties of a noble gas superatom or an alkali superatom, respectively [7, 9, 22-23]. While the Al central atom substituted by a Cu atom, it is analogous to a phosphorus atom [24]. The similar situation occurs in the Frank-Kasper structure $M@Si_{16}$ by encapsulating metal atom into Si_{16} cage [25-28], and also in nanoclusters $M@B_n$ [29], $M@Au_{12}$ [30], and $M@Sn_n$ [31-32], etc.

Motivated by the results of fusion a hetero-atom into an outer cage to tailor their properties, we here select lithium clusters as prototypes to extend the existing conclusions. Lithium is the lightest metal and possesses a simple electronic shell of

($1s^2 2s^1$). More importantly, it tends to form compact structures, being a good starting. Base on this points, we recently design a series of D_{6d} symmetry tetrahexahedral superatoms $TM@Li_{14}$ (TM=Sc, Ti, V, Y, Zr, Nb, Hf, Ta, and W), where the selected transition-metal atom is embedded at the center of cage composed by the fourteen lithium atoms [21]. Further, a new face-sharing bi-tetrahexahedral mode $M_1M_2@Li_{20}$ (M_1, M_2= Ti and W) is assembled from the tetrahexahedral superatoms $Ti@Li_{14}$ and $W@Li_{14}$ [33]. It is an interesting challenge to form the molecules and bulk crystals by direct connection or partial fusion of clusters, which in most case are prone to coalesce. So far, three different bonding modes assembled from superatoms have been revealed in ligand-protected Au superatomic molecules, i.e. the vertex-sharing [34], face-sharing [35-36], and nonsharing modes [37-38], which are not further discussed here for the purpose of designing superatoms.

However, there should be other lithium binary superatoms with high coordination numbers (N>12). Research of $TM@Li_{14}$ cluster suggests that the lowest energy isomer is cage-like structure only if the number of valence electrons is less than 20. Within this range, lithium binary superatoms can be formed even if they are with an odd number electrons [19, 21], where the stability can be obtained by spin multiplicities or by undergoing spatial distortions to form a large gap state [39]. In this regard, a series of transition-metal elements are respectively embedded into Li_{15} cage. By the search of particle swarm optimisation algorithm (PSO), a D_{3h} symmetry core-shell superatoms $TM@Li_{15}$ (TM=Sc, Ti, Y, Zr, Nb, Hf, and Ta) are found, where the outer cage is composed by the fifteen lithium atoms and the hetero transition-metal atom is

centered. The stability of TM@Li_{15} (TM=Sc, Ti, Y, Zr, Nb, Hf, and Ta) is discussed from the aspects of geometric structures, electronic shells, the energy, magnetic properties, and the energy gaps in the following.

2. COMPUTATIONAL METHODS

The search of the low energy structures of TM@Li_{15} (TM=Sc, Ti, V, Y, Zr, Nb, Hf, and Ta) clusters are completed through Crystal structure AnaLYsis by Particle Swarm Optimization (CALYPSO) [40]. Then, the obtained first five low energy structures are re-optimized by density-functional theory (DFT) calculations implemented in the Gaussian16 package [41]. To give reasonable results, the assessment of density functionals for transition-metal compounds are consulted [42-44] and three proved valid functionals, namely, pure functional PW91 [45], meta-GGA functional M06-L [46], and hybrid functional TPSSH [47], are selected. SDD is chosen as the basis set [48]. Also, the gap of Li_{16} cluster is calculated by these three functionals listed in Table 2, where the values obtained from PW91 and M06-L functionals are agreed well with that of the theoretical result of Fournier et al. [49]. Moreover, considering the use of PW91 functional in VLi_n (n=1-13) clusters studies [19], we select the PW91 functional to carry out most results. All the low energy isomers are confirmed as true local minima for there are without any imaginary values by frequencies calculations. Moreover, the spin multiplicities (SMs) of each isomer is identified, where the SM of isomer with the lowest total energy is delivered to the ground state. Molecular visualization is completed by Multiwfn_3.6 [50].

3. RESULTS AND DISCUSSION

Aiming for discovering stable superatoms, the whole 3d transition-metal atoms are respectively doped into Li_{15} cage forming a cluster with the assigned compositions, namely $TM@Li_{15}$. Through CALYPSO structure prediction method, we obtain a D_{3h} symmetry cage-like isomer centered with Sc or Ti atom as the global minimum, which is shown in Figure 1 (A). The unique structure of $TM@Li_{15}$ with D_{3h} symmetry can be obtained by relaxation of the fourteen-coordinate $TM@Li_{14}$ clusters, of which a topped lithium atom of the C_6 axis is replaced by a pair of symmetry capping lithium atoms along the vertical axial direction. From table 1, we can see that there is a fluxional behavior among the low energy isomers of lithium clusters. Especially, the other low energy isomers have a tendency to become the isomer A due to the high mobility of lithium. Such a combination can be extended to the same main group, i.e. Y, Zr, or Hf atoms as dopants. On basis of the jellium model, the 20-electron $TM@Li_{15}$ clusters are supposed to be existing. However, the lowest energy isomer with the D_{3h} symmetry is only found doped with Nb or Ta atom except V element, which may be due to the mismatch of atomic radius. As expected, other 3d transition-metal atoms (TM=Cr, Mn, Fe, Co, Ni, Cu) encapsulated into the Li_{15} cage, the global minimum are not the D_{3h} symmetry cage-like structures, similar to the situation of $TM@Li_{14}$ [21]. Thus, these results are not shown.

The stability of $TM@Li_{15}$ (TM=Sc, Ti, Y, Zr, Nb, Hf, and Ta) clusters with the D_{3h} symmetry is further determined by the average binding energy (E_b) per atom and the fragmentation energy (E_f), which are respectively defined as the following formulas:

$$E_b\left(TM\ @\ Li_{15}\right)=\frac{E(TM)+15E(Li)-E\left(TM\ @\ Li_{15}\right)}{16}$$

$$E_f\left(TM@Li_{15}\right)=E(TM@Li_{14})+E(Li)-E(TM@Li_{15})$$

In the above formulas, TM represents transition-metal atoms Sc, Ti, Y, Zr, Nb, Hf, and Ta. E(TM@Li_{15}) represents the total energy of TM@Li_{15} with D_{3h} symmetry, and E(TM@Li_{14}) is the total energy of its fragment formed by one lithium detached from TM@Li_{15}. E(Li) and E(TM) represent the total energy of the free state Li element and the free state dopants, respectively. Moreover, for the cage clusters, the interaction of an embedded element and the outer shell, namely the embedding energy, is needed to be considered, which indicates the feasibilities of fusion of a transition-metal atom into Li_{15} cage. The embedding energy of TM@Li_{15} (TM=Sc, Ti, Y, Zr, Nb, Hf, and Ta) can be calculated as following:

$$D_e\left(TM@Li_{15}\right)=(E(\text{shell})+E(\text{core}))-E\left(TM@Li_{15}\right)$$

Where the total energies of the outer shell, the embedded transition-metal element, and the whole cluster are denoted as E(shell), E(core) and E(TM@Li_{14}), respectively. Using such definition, a positive D_e value means that the dopants can be encapsulated into the Li_{15} cage.

The results of energy calculations are shown in Table 2 and plotted in Figure 2 for clarity. It can be seen from Figure 2 that the trends of TM@Li_{15} (TM=Sc, Ti, Y, Zr, Nb, Hf, and Ta) calculated by the three functionals are consistent except the difference of Hf@Li_{15}, where E_b of Hf@Li_{15} from the calculation of TPSSH is higher than that of Nb@Li_{15} and Ta@Li_{15}, in contradiction to the results of PW91 and M06-L functionals. However, it doesn't affect our concern that Hf@Li_{15} is stable. With the variation of

dopants in succession, the overall trend of E_b is upward for the D_{3h} symmetry $TM@Li_{15}$ (TM=Sc, Ti, Y, Zr, Nb, Hf, and Ta) clusters. Whereas their fragmentation energies decrease monotonically with the comparison between the same period elements as dopants, indicating the stability reduced successively. The features of E_b and E_f of $TM@Li_{15}$ are similar to our previous superatoms $TM@Li_{14}$ [21]. Moreover, the positive values of D_e show the feasibilities of encapsulating the chosen elements (TM=Sc, Ti, Y, Zr, Nb, Hf, and Ta) into Li_{15} cage, where a larger D_e is more suitable to implant.

The energy gaps (E_{gap}) of $TM@Li_{15}$ (TM=Sc, Ti, Y, Zr, Nb, Hf, and Ta) are also examined, which are defined as the energy differences of the highest occupied molecular orbital (HOMO) and the lowest unoccupied molecular orbital (LUMO). Researches show that the stability of a small cluster can be enhanced with a large gap. As shown in Table 2 and Figure 3, the HOMO-LUMO gaps of $TM@Li_{15}$ (TM=Sc, Ti, Y, Zr, Nb, Hf, and Ta) clusters are from 0.20 eV to 1.10 eV under the PW91/SDD calculations. The values of these gaps, especially of $TM@Li_{15}$ (TM=Ti, Zr, and Hf), seem to be smaller compared with that of Al_{13}^- (1.87 eV) [51]. However, taking the gaps of typical magnetic superatoms as references, such as $Sc@K_{12}$ (0.35 eV) [17], $Mn@Sr_9$ (0.39 eV) [18], and $V@Na_8$ (0.42 eV) [20], etc., these gaps are reasonable. In addition, a more accurate gap is given by the calculation of TPSSH hybrid functional jointing SDD basis set for the standard GGA, such as PW91 and M06-L functionals, have the tendency of underestimating the gaps. Note the gaps of 20-electron $Nb@Li_{15}$ and $Ta@Li_{15}$ are obviously larger than that of other $TM@Li_{15}$,

which maybe help reduce the instability causing by their small fragmentation energies. The similar situation occurs in the $TM@Li_{15}$, where the gap of $W@Li_{15}$ is significant larger than others', further enhancing its stability.

To study the origins of their stability, the role of geometric and electronic shells need be focused for they have an important effect on the stability of small clusters [39, 52]. Obviously, all the lowest energy isomers of $TM@Li_{15}$ (TM=Sc, Ti, Y, Zr, Nb, Hf, and Ta) are with the geometric shell closures due to their cage-like shapes, and the high symmetry usually lead to even charge distribution with the reduction of their reactivity. Therefore, the electronic shells are crucial to their stability. In the following, their one electron levels and associated Kohn-Sham molecular orbitals (MOs) will be analyzed. For the sake of discussion, $TM@Li_{15}$ (TM=Sc, Ti, and Nb) are chosen as the representative clusters, where the properties of $TM@Li_{15}$ (TM= Y, Zr, Hf, and Ta) are analogy to that of the corresponding representative clusters.

For $Sc@Li_{15}$, the number of valance electrons is 18, where a $3d^14s^2$ and $2s^1$ electrons are offered by a scandium atom and each lithium atom, respectively. One electron energy levels and MOs diagram of $Sc@Li_{15}$ are given in Figure 4. By comparing its orbitals shapes and nodes with that of atom, the lowest state is identified as 1S for it is spread out over the whole cluster. The next three states have $1P_x$, $1P_y$ and $1P_z$ characteristics, where the degeneracy of the 1P orbitals is broken into two sets due to the oblate shape of the cluster, and the $1P_z$ orbital is 0.20 eV lower in energy. Also, the splitting of degenerate orbitals occurs in the five degenerate 1D orbitals forming two groups with 3 and 2 orbitals, since the oblate structure leads to

the characteristic of the crystal field. Thus, the filling order of $Sc@Li_{15}$ is $1S^21P^61D^{10}$, with a closed electronic shell. On the basis of the jellium model, the 18-electron $Sc@Li_{15}$ is high stable. The similar situation happens for $Nb@Li_{15}$ cluster, where five effective valance electrons ($4d^45s^1$) are offered by a niobium atom and others are from the lithium atom of $2s^1$ electron. As shown in Figure 4, the two more electrons of $Nb@Li_{15}$ locate in 2S orbital, and thus the filling configuration of valance electrons is $1S^21P^61D^{10}2S^2$, fulfilling the 20-electron rule. Also, the electronic shell of $Nb@Li_{15}$ is closed, possessing high stability. With all the electrons paired, both $Sc@Li_{15}$ and $Nb@Li_{15}$ are nonmagnetic superatoms.

Unlike $Sc@Li_{15}$ and $Nb@Li_{15}$ superatoms, $Ti@Li_{15}$ has an odd number of effective valence electrons, where 4 electrons are offered by a titanium atom ($3d^24s^2$) and 15 electrons from lithium atoms ($2s^1$). However, the 19-electron $Ti@Li_{15}$ is not corresponding to a magic cluster. With a partially filled subshell, the stability of $Ti@Li_{15}$ can be imparted via a spin multiplicity. The energy level correlation and MOs diagram of $Ti@Li_{15}$ are also presented in Figure 4, where the MOs of spin up and spin down electrons are splitting into two levels due to its open electronic shell. The first nine orbitals of $Ti@Li_{15}$, including the 1S, 1P, and 1D orbitals, are occupied by the paired electrons, while the extra one single electron is filling $2S_\alpha^1$ orbital. The corresponding superatomic configuration of $Ti@Li_{15}$ is $1S^21P^61D^{10}2S_\alpha^1$, with a spin magnetic moment of 1.0 μ_B.

Through fusing a transition-metal element (TM=Sc, Ti, Y, Zr, Nb, Hf, and Ta) into Li_{15} cage, the D_{3h} symmetry superatoms $TM@Li_{15}$ are formed. Their stability can be

well understood based on the superatoms and the magnetic superatoms models. For $TM@Li_{15}$ (TM=Sc, Y, Nb, and Ta), they are all with the closed electronic shells, fulfilling the 18-electron and 20-electron rules, respectively. Doped by a transition-metal atom Ti, Zr, and Hf, the stability of 19-electron $TM@Li_{15}$ is acquired though the formation of magnetic superatom with a spin magnetic moment of 1 μ_B. This finding is developing the binary superatoms family, and also is an extension of $TM@Li_{14}$ (TM = Sc, Ti, V, Y, Zr, Nb, Hf, Ta and W) [21]. With an addition of lithium atom, the core will handle a more atom and the cage-like structure retained will be more difficult. Due to the effective valence electrons increasement of one, the variations of total magnetic moments are $1\mu_B$. Based on the superatoms and magnetic superatoms models, more superatoms can be designed. Further, the functional materials with tailored features will be assembled from superatoms in potential applications.

4. CONCLUSIONS

Through encapsulating a transition-metal atom (TM=Sc, Ti, Y, Zr, Nb, Hf, and Ta) into the Li_{15} cage, the D_{3h} symmetry transition-metal-doped superatoms $TM@Li_{15}$ are formed, where the transition-metal element is at the center of Li_{15} cage. The unique structure is the lowest energy isomer located by particle swarm optimization implanted in the CALYPSO package. Based on the superatom and the magnetic superatom models, their stability can be well analyzed. For $Sc@Li_{15}$ and $Nb@Li_{15}$, the valance electronic filling orders are $1S^21P^61D^{10}$ and $1S^21P^61D^{10}2S^2$, fulfilling the

18-electron and the 20-electron rules, respectively. As for $Ti@Li_{15}$, its characteristic order is $1S^21P^61D^{10}2S_\alpha^1$, with a spin magnetic moment of 1.0 μ_B. Due to the dopants with same effective valance electrons, the filling orders of $TM@Li_{15}$ (TM=Y, Zr, Hf, and Ta) are similar to $TM@Li_{15}$ (TM=Sc, Ti, and Nb), respectively. The stability of $TM@Li_{15}$ (TM=Sc, Ti, Y, Zr, Nb, Hf, and Ta) is also confirmed by energy calculations. Moreover, the moderate HOMO-LUMO gaps further enhance their stability. According to the superatoms and magnetic superatoms models, more stable clusters can be designed, which will offer abundant building units to assemble functional materials and devices for real-life applications in future.

CONFLICT OF INTEREST

The authors declare that they have no conflict of interest.

ACKNOWLEDGMENT

This work is supported by the Special Foundation for Theoretical Physics Research Program of China (No.11847119).

REFERENCES

[1] Khanna S N, and Jena P 1995 Atomic Clusters: Building Blocks for a Class of Solids *Phys. Rev. B* 51 13705-13716.

[2] Castleman A W, and Khanna S N 2009 Clusters, Superatoms, and Building Blocks of New Materials *J. Phys. Chem. C* 113 2664–2675.

[3] Claridge S A, Castleman A W, Khanna S N, Murray C B, Sen A, and Weiss P S 2009 Cluster-Assembled Materials *ACS Nano* 3 244–255.

[4] Aoyagi S, et al. 2010 A Layered Ionic Crystal of Polar $Li@C_{60}$ Superatoms *Nat. Chem.* 2 678-83.

[5] Mandal S, Reber A C, Qian M, Weiss P S, Khanna S N, and Sen A 2013 Controlling the Band Gap Energy of Cluster-Assembled Materials *Acc. Chem. Res.* 46 2385-2395.

[6] Zhang J, Rowland C, Liu Y, Xiong H, Kwon S, Shevchenko E, Schaller R D, Prakapenka V B, Tkachev S, and Rajh T 2015 Evolution of Self-Assembled ZnTe Magic-Sized Nanoclusters *J. Am. Chem. Soc.* 137 742-749.

[7] Reber A C, Khanna S N, and Castleman A W 2007 Superatom Compounds, Clusters, and Assemblies: Ultra Alkali Motifs and Architectures *J. Am. Chem. Soc.* 129 10189-10194.

[8] Dodabalapur A, Katz H E, Torsi L, and Haddon R C 1995 Organic Heterostructure Field-Effect Transistors *Science* 269 1560-1562.

[9] Meijer E J, de Leeuw D M, Setayesh S, van Veenendaal E, Huisman B H, Blom P W, Hummelen J C, Scherf U, Kadam J, and Klapwijk T M 2003 Solution-Processed Ambipolar Organic Field-Effect Transistors and Inverters *Nat. Mater.* 2 678-682.

[10] Yu G, Gao J, Hummelen J C, Wudl F, and Heeger A J 1995 Polymer Photovoltaic Cells: Enhanced Efficiencies Via a Network of Internal Donor-Acceptor Heterojunctions *Science* 270 1789-1791.

[11] Li G, Shrotriya V, Huang J, Yao Y, Moriarty T, Emery K, and Yang Y 2005 High-Efficiency Solution Processable Polymer Photovoltaic Cells by Self-Organization of Polymer Blends *Nat. Mater.* 4 864-868.

[12] Yong Y, Jiang H, Li X, Lv S, and Cao J 2016 The Cluster-Assembled Nanowires Based on $M_{12}N_{12}$ (M = Al and Ga) Clusters as Potential Gas Sensors for Co, No, and No2 Detection *Phys. Chem. Chem. Phys.* 18 21431-21441.

[13] Bergeron D E, Castleman A W, Morisato T, and Khanna S N 2004 Formation of $Al_{13}I^-$: Evidence for the Superhalogen Character of Al_{13} *Science* 304 84-87.

[14] Ekardt W 1984 Work Function of Small Metal Particles: Self-Consistent Spherical Jellium-Background Model *Phys. Rev. B* 29 1558-1564.

[15] Ekardt W 1986 Theory of Electronic Excitations in Coated Metal Particles: Jellium-on-Jellium Model *Phys. Rev. B* 34 526-533.

[16] Reveles J U, Clayborne P A, Reber A C, Khanna S N, Pradhan K, Sen P, and Pederson M R 2009 Designer Magnetic Superatoms *Nat. Chem.* 1 310-315.

[17] Pradhan K, Reveles J U, Sen P, and Khanna S N 2010 Enhanced Magnetic Moments of Alkali Metal Coated Sc Clusters: New Magnetic Superatoms *J. Chem. Phys.* 132 124302.

[18] Medel V, Reveles J U, and N. Khanna S N 2012 Magnetism of Electrons in Atoms and Superatoms *J. Appl. Phys.* 112 064313.

[19] Zhang M, Zhang J, Feng X, Zhang H, Zhao L, Luo Y, and Cao W 2013 Magnetic Superatoms in VLi_n (N = 1-13) Clusters: A First-Principles Prediction *J. Phys. Chem. A* 117 13025-13036.

[20] Zhang X, Wang Y, Wang H, Lim A, Gantefoer G, Bowen K H, Reveles J U, and Khanna S N 2013 On the Existence of Designer Magnetic Superatoms *J. Am. Chem. Soc.* 135 4856-4861.

[21] Yan L, Liu J, and Shao J 2019 Superatomic Properties of Transition-Metal-Doped Tetrahexahedral Lithium Clusters: $TM@Li_{14}$ *Mol. Phys.* Doi: 10.1080/00268976.2019.1592256.

[22] Molina B, Soto J R, and Castro J J 2012 Stability and Nonadiabatic Effects of the Endohedral Clusters $X@Al_{12}$ (X = B, C, N, Al, Si, P) with 39, 40, and 41 Valence Electrons *J. Phys. Chem. C* 116 9290-9299.

[23] Gong X G, and Kumar V V 1993 Enhanced Stability of Magic Clusters: A Case Study of Icosahedral $Al_{12}X$, X=B, Al, Ga, C, Si, Ge, Ti, As *Phys. Rev. Lett.* 70 2078-2081.

[24] Reveles J U, Baruah T, and Zope R R 2015 $Al_{12}Cu$ Superatom as Stable Building Block of Ionic Salts *J. Phys. Chem. C* 119 5129-5137.

[25] Shibuta M, Ohta T, Nakaya M, Tsunoyama H, Eguchi T, and Nakajima A 2015 Chemical Characterization of an Alkali-Like Superatom Consisting of a Ta-Encapsulating Si_{16} Cage *J. Am. Chem. Soc.* 137 14015-14018.

[26] Koyasu K, Akutsu M, Mitsui M, and Nakajima A 2005 Selective Formation of MSi_{16} (M=Sc, Ti, and V) *J. Am. Chem. Soc.* 127 4998-4999.

[27] Tsunoyama H, Akatsuka H, Shibuta M, Iwasa T, Mizuhata Y, Tokitoh N, and Nakajima A 2017 Development of Integrated Dry–Wet Synthesis Method for Metal Encapsulating Silicon Cage Superatoms of M@Si_{16} (M = Ti and Ta) *J. Phys. Chem. C* 121 20507-20516.

[28] Kumar V, Majumder C, and Kawazoe Y 2002 M@Si_{16}, M=Ti, Zr, Hf: P Conjugation, Ionization Potentials and Electron Affinities *Chem. Phys. Lett.* 363 319–322.

[29] Zhai H J, et al. 2014 Observation of an All-Boron Fullerene *Nat. Chem.* 6 727-731.

[30] Zhai H J, Li J, and Wang L S 2004 Icosahedral Gold Cage Clusters: M@Au_{12}^- (M=V, Nb, and Ta) *J. Chem. Phys.* 121 8369-8374.

[31] Atobe J, Koyasu K, Furuse S, and Nakajima A 2012 Anion Photoelectron Spectroscopy of Germanium and Tin Clusters Containing a Transition- or Lanthanide-Metal Atom; MGe_n^- (n = 8-20) and Msn_n^- (n= 15-17) (M = Sc-V, Y-Nb, and Lu-Ta) *Phys. Chem. Chem. Phys.* 14 9403-9410.

[32] Cui L F, Huang X, Wang L M, Zubarev D Y, Boldyrev A I, Li J, and Wang L S 2006 Sn122-: Stannaspherene *J. Am. Chem. Soc.* 128 8390-8391.

[33] Yan L 2019 Face-Sharing Homo- and Hetero-Bitetrahexahedral Superatomic Molecules M_1M_2@Li_{20} (M_1/M_2 = Ti and W) *J. Phys. Chem. A* 123 5517-5524.

[34] Nobusada K, and Iwasa T 2007 Oligomeric Gold Clusters with Vertex-Sharing Bi- and Triicosahedral Structures *J. Phys. Chem. C* 111 14279-14282.

[35] Cheng L, Ren C, Zhang X, and Yang J 2013 New Insight into the Electronic Shell of $Au_{38}(SR)_{24}$: A Superatomic Molecule *Nanoscale* 5 1475-1488.

[36] Qian H, Eckenhoff W T, Zhu Y, Pintauer T, and Jin R 2010 Total Structure Determination of Thiolate-Protected Au_{38} Nanoparticles *J. Am. Chem. Soc.* 132 8280–8281.

[37] Qian H, Zhu Y, and Jin R 2010 Isolation of Ubiquitous $Au_{40}(SR)_{24}$ Clusters from the 8 KDa Gold Clusters. *J. Am. Chem. Soc.* 132 4583–4585.

[38] Malola S, Lehtovaara L, Knoppe S, Hu K-J, Palmer R E, Bürgi T, and Häkkinen H 2012 $Au_{40}(SR)_{24}$ Cluster as a Chiral Dimer of 8-Electron Superatoms: Structure and Optical Properties *J. Am. Chem. Soc.* 134 19560-19563.

[39] Reber A C, and Khanna S N 2017 Superatoms: Electronic and Geometric Effects on Reactivity *Acc. Chem. Res.* 50 255-263.

[40] Lv J, Wang Y, Zhu L, and Ma Y 2012 Particle-Swarm Structure Prediction on Clusters *J. Chem. Phys.* 137 084104.

[41] Frisch M J, Trucks G W, Schlegel H B, Scuseria G E, Robb M A, Cheeseman J R, Scalmani G, Barone V, Mennucci B, and Petersson G A e 2016 Gaussian 16, Revision B.01 *Gaussian, Inc.:Wallingford, Ct*.

[42] Dohm S, Hansen A, Steinmetz M, Grimme S, and Checinski M P 2018 Comprehensive Thermochemical Benchmark Set of Realistic Closed-Shell Metal Organic Reactions *J. Chem. Theory Comput.* 14 2596-2608.

[43] Weymuth T, Couzijn E P, Chen P, and Reiher M 2014 New Benchmark Set of Transition-Metal Coordination Reactions for the Assessment of Density Functionals *J. Chem. Theory Comput.* 10 3092-3103.

[44] Goerigk L, Hansen A, Bauer C, Ehrlich S, Najibi A, and Grimme S 2017 A Look at the Density Functional Theory Zoo with the Advanced Gmtkn55 Database for General Main Group Thermochemistry, Kinetics and Noncovalent Interactions *Phys. Chem. Chem. Phys.* 19 32184-32215.

[45] Perdew J P, and Wang Y 1992 Accurate and Simple Analytic Representation of the Electron-Gas Correlation Energy *Phys. Rev. B* 45 13244-13249.

[46] Zhao Y, and Truhlar D G 2006 A New Local Density Functional for Main-Group Thermochemistry,

Transition Metal Bonding, Thermochemical Kinetics, and Noncovalent Interactions *J. Chem. Phys.* 125 194101.

[47] Viktor N S, Gustavo E S, Jianmin T, and John P P 2003 Comparative Assessment of a New Nonempirical Density Functional: Molecules and Hydrogen-Bonded Complexes *J. Chem. Phys.* 119 12129.

[48] Hay P J, and Wadt W R 1985 Ab Initio Effective Core Potentials for Molecular Calculations. Potentials for the Transition Metal Atoms Sc to Hg *J. Chem. Phys.* 82 270-283.

[49] Fournier R, Bo Yi Cheng J, and Wong A 2003 Theoretical Study of the Structure of Lithium Clusters *J. Chem. Phys.* 119 9444-9454.

[50] Lu T, and Chen F 2012 Multiwfn: A Multifunctional Wavefunction Analyzer *J. Comput. Chem.* 33 580-92.

[51] Khanna S N, Rao B K, and Jena P 2002 Electronic Signature of the Magicity and Ionic Bonding In $Al_{13}X$ (X=Li–K)Clusters *Phys. Rev. B* 65.

[52] Luo Z, and Castleman A W 2014 Special and General Superatoms *Acc. Chem. Res.* 47 2931-40.

Table 1. Relative energies of TM@Li_{15} (TM=Sc, Ti, V, Y, Zr, Nb, Hf, and Ta), of which the selected references with 0.00 eV are the total energies of their own lowest-energy isomers. The letters A to E correspond to the first five low energy isomers presented in Fig. 1

TM	A	B	C	D	E
Sc	0	A	A	A	A
Y	0	A	A	A	A
Ti	0	A	0.22	A	0.67
Zr	0	A	0.38	A	1.13
Hf	0	A	A	A	1.25
V	0.28	0.34	0.32	0.48	0
Nb	0	A	0.08	A	0.66
Ta	0	A	0.27	A	0.97

Table 2. Symmetry, Fragmentation Energy (E_f), Average Binding Energy (E_b) Per Atom, Embedding Energy (D_e), HOMO-LUMO Gaps (E_{gap}) and Total Magnetic Moment (μ_s) of TM@Li_{15} (TM=Sc, Ti, Y, Zr, Nb, Hf, and Ta) calculated by Gaussian 16. *Li_{16} is proved as a superatomic molecule.

Cluster(TM@Li_{15})		Symm.	E_f(eV)	E_b(eV)	D_e(eV)	E_{gap}(eV)	μ_s(μB)
Sc	PW91	D_{3h}	1.54	1.28	4.20	0.40	0
	M06L		1.63	1.39	4.55	0.34	
	TPSSH		1.53	1.26	3.84	0.81	
Y	PW91	D_{3h}	1.73	1.32	4.87	0.56	0
	M06L		1.82	1.44	5.42	0.53	
	TPSSH		1.73	1.32	4.87	1.00	
Ti	PW91	D_{3h}	1.26	1.41	6.20	0.26	1
	M06L		1.34	1.49	6.11	0.25	
	TPSSH		1.16	1.35	5.26	0.51	
Zr	PW91	D_{3h}	1.29	1.50	7.65	0.20	1
	M06L		1.38	1.58	7.65	0.20	

	TPSSH		1.21	1.47	7.31	0.53	
Hf	PW91	D_{3h}	1.44	1.47	7.27	0.21	1
	M06L		1.55	1.57	7.49	0.21	
	TPSSH		1.40	1.46	7.03	0.56	
Nb	PW91	D_{3h}	1.06	1.49	7.45	0.87	0
	M06L		1.14	1.53	6.85	0.86	
	TPSSH		0.94	1.48	7.36	1.21	
Ta	PW91	D_{3h}	1.24	1.49	7.57	1.10	0
	M06L		1.34	1.54	6.93	1.11	
	TPSSH		1.16	1.51	7.80	1.47	
Li_{16}*	PW91	C_{2v}	1.47	1.11	-	0.44	3
	M06L		1.58	1.20	-	0.40	
	TPSSH		1.45	1.11	-	0.85	

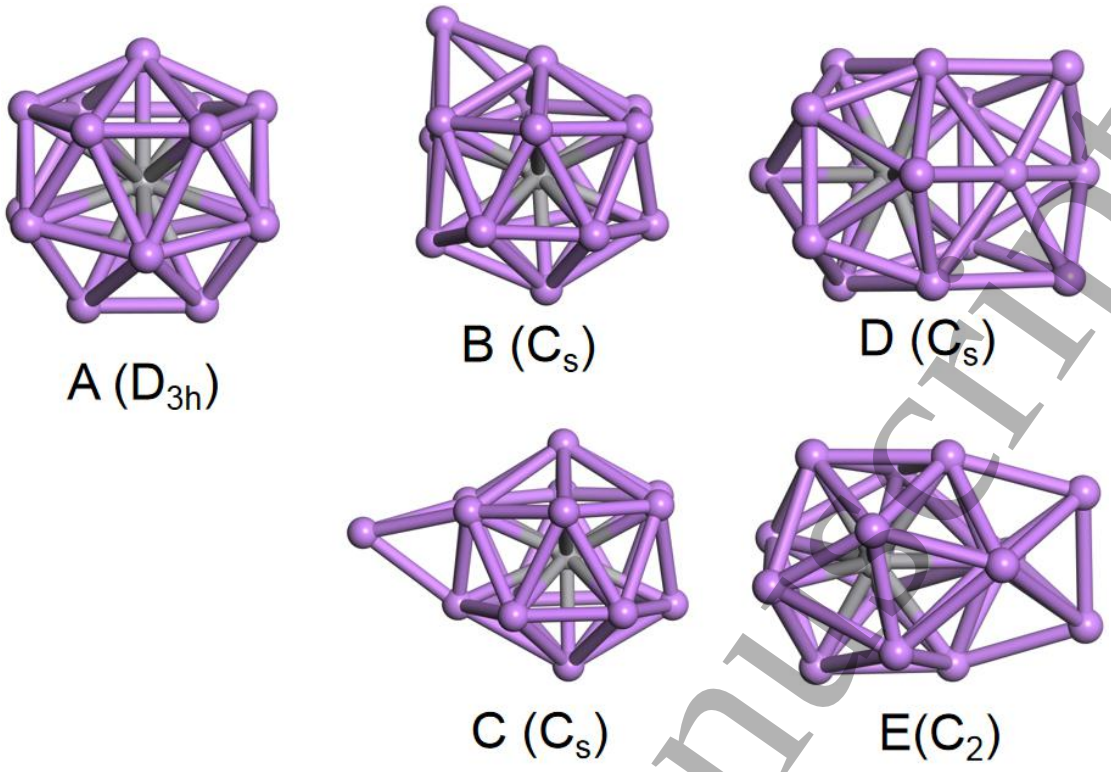

Figure 1. The lowest-energy and low-lying isomers of $TM@Li_{15}$ (TM=Sc, Ti, V, Y, Zr, Nb, Hf, and Ta) are shown. The gray atoms are dopants and lithium atoms are purple. A: along threefold axis, a capping lithium atom of the D_{6d} symmetry $TM@Li_{14}$ is replaced by a pair of lithium in the horizontal plane.

B: a lithium atom is added at the top of C_6 axis of D_{6d} symmetry $TM@Li_{14}$.

C: along the vertical axis direction, an addition of lithium atom is on the surface of the D_{6d} symmetry $TM@Li_{14}$.

D: three lithium atoms are away from the core.

E: two lithium atoms are away from the core.

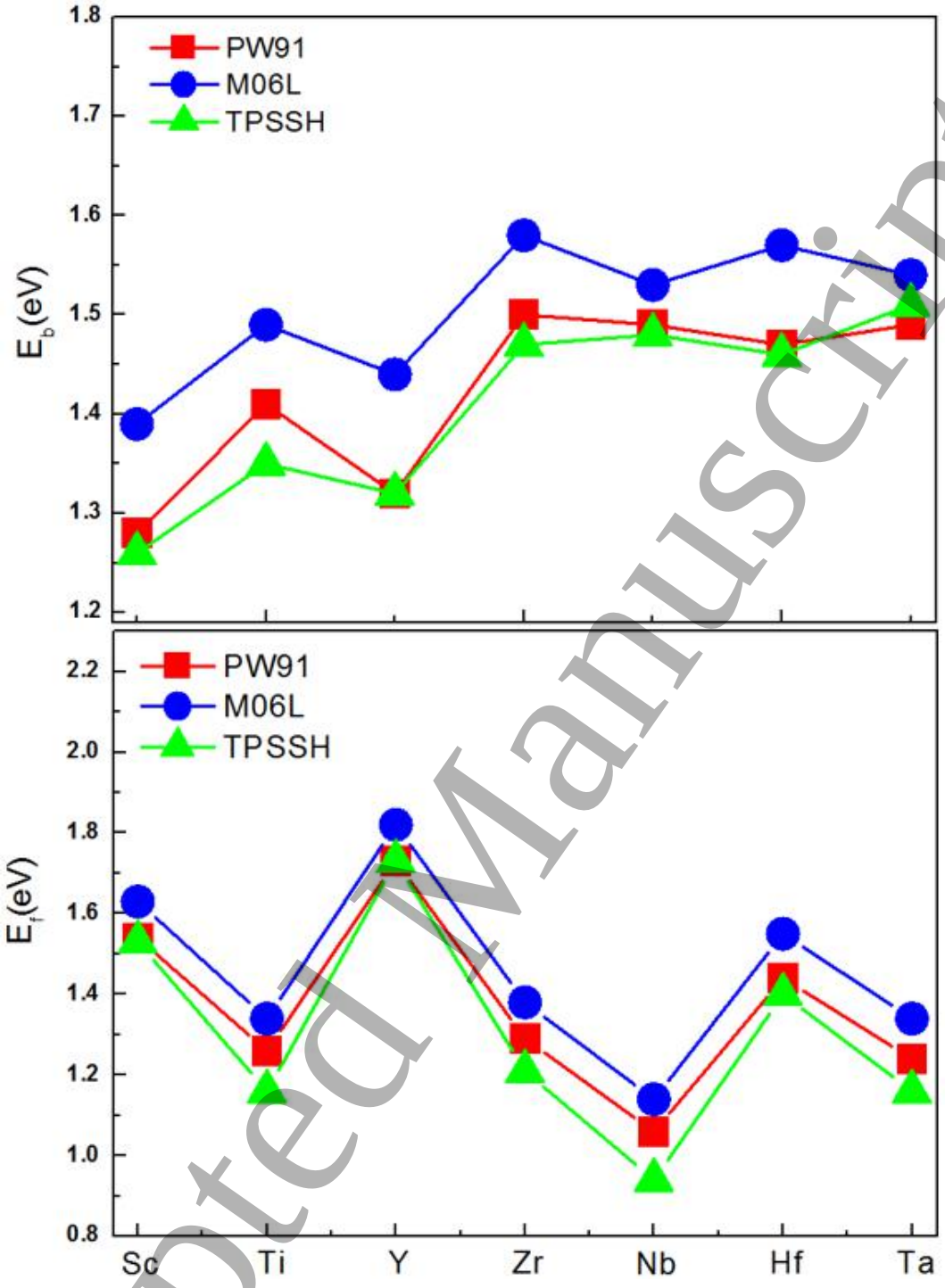

Figure 2. The diagrams of average binding energies per atom (E_b) and fragmentation energies (E_f) of TM@Li_{15} (TM=Sc, Ti, Y, Zr, Nb, Hf, and Ta) with the lowest energy.

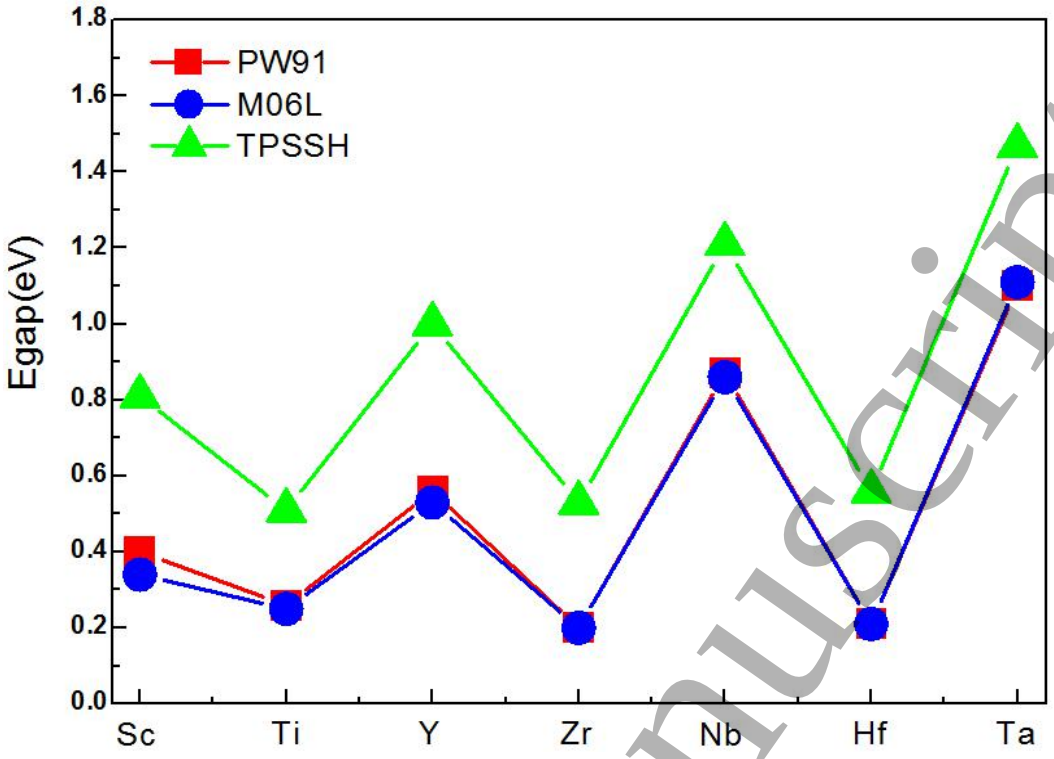

Figure 3. The graphic of HOMO-LUMO energy gap (E_{gap}) of TM@Li_{15} (TM=Sc, Ti, Y, Zr, Nb, Hf, and Ta) with the lowest energy.

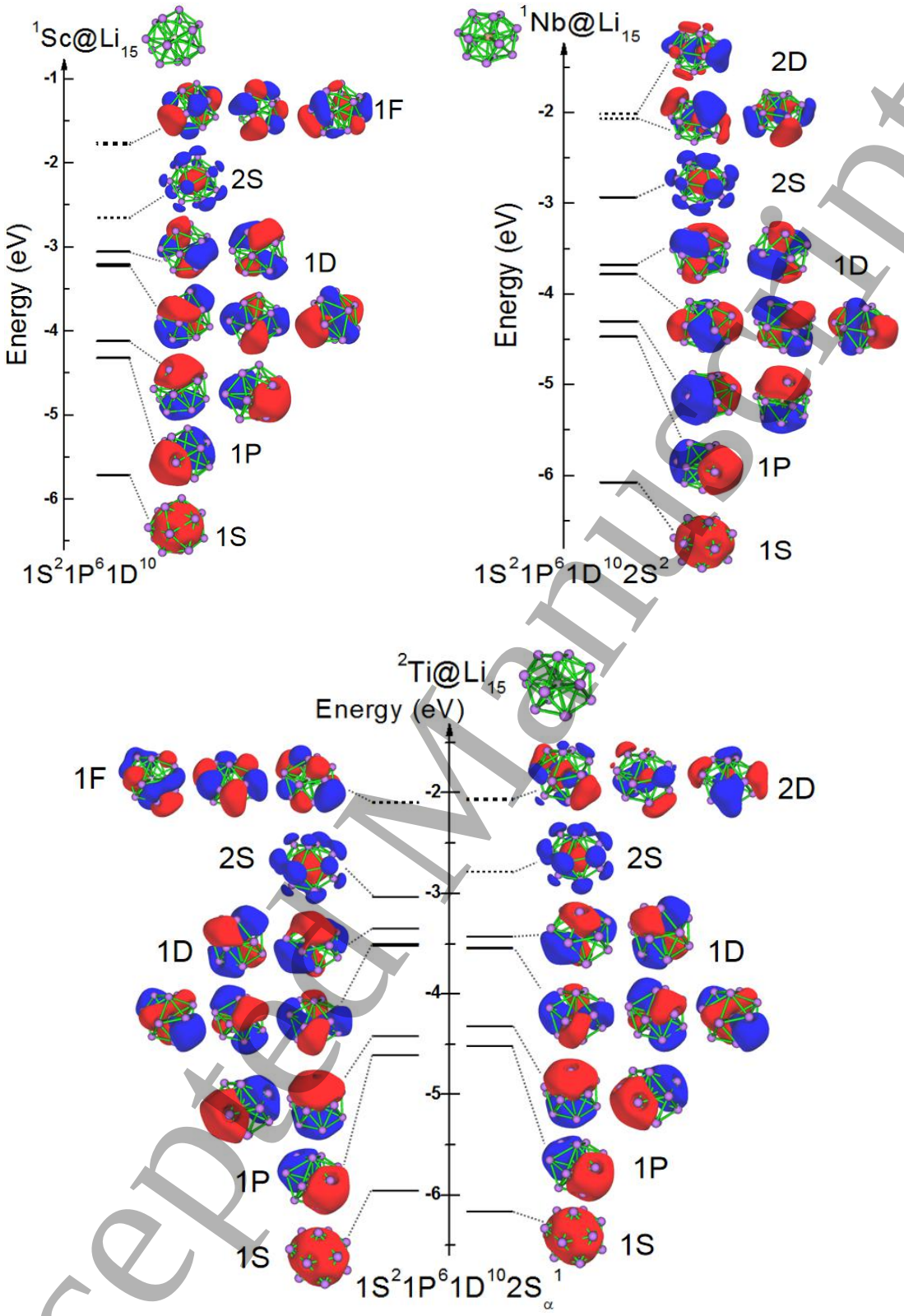

Figure 4. One electron energy levels and MOs of the representative superatoms $TM@Li_{15}$ (TM=Sc, Ti, and Nb). Continuous lines are the filled levels while the dotted

lines correspond to the unfilled states. For each level, the degenerated energy states are arranged in a horizontal line. The surface isovalue of MO plotting is 0.022 e/Å^3.